HHS Public Access

Author manuscript

Med Phys. Author manuscript; available in PMC 2021 November 01.

Published in final edited form as:

Med Phys. 2020 November ; 47(11): 5428–5440. doi:10.1002/mp.14491.

Intensity-Modulated Proton Therapy (IMPT) Interplay Effect Evaluation of Asymmetric Breathing with Simultaneous Uncertainty Considerations in Patients with Non-Small Cell Lung Cancer

Jie Shan, MS[1,*], **Yunze Yang, PhD**[1,*], **Steven E. Schild, MD**[1], **Thomas B. Daniels, MD**[1], **William W. Wong, MD**[1], **Mirek Fatyga, PhD**[1], **Martin Bues, PhD**[1], **Terence T. Sio, MD, MS**[1], **Wei Liu, PhD**[1]

[1]Department of Radiation Oncology, Mayo Clinic, Phoenix, AZ, 85054, USA.

Abstract

Purpose: Intensity-modulated proton therapy (IMPT) is sensitive to uncertainties from patient setup and proton beam range, as well as interplay effect. In addition, respiratory motion may vary from cycle to cycle, and also from day to day. These uncertainties can severely degrade the original plan quality and potentially affect patient's outcome. In this work, we developed a new tool to comprehensively consider the impact of all these uncertainties and provide plan robustness evaluation under them.

Methods: We developed a comprehensive plan robustness evaluation tool that considered both uncertainties from patient setup and proton beam range, as well as respiratory motion simultaneously. To mimic patients' respiratory motion, the time spent in each phase was randomly sampled based on patient-specific breathing pattern parameters as acquired during the 4D-CT simulation. Spots were then assigned to one specific phase according to the temporal relationship between spot delivery sequence and patients' respiratory motion. Dose in each phase was calculated by summing contributions from all the spots delivered in that phase. The final 4D dynamic dose was obtained by deforming all doses in each phase to the maximum exhalation phase. Three hundred (300) scenarios (10 different breathing patterns with 30 different setup and range uncertainty scenario combinations) were calculated for each plan. The dose-volume histograms (DVHs) band method was used to assess plan robustness. Benchmarking the tool as an application's example, we compared plan robustness under both 3D and 4D robustly optimized IMPT plans for 10 non-randomly selected patients with non-small cell lung cancer.

Corresponding Author: Wei Liu, PhD, Associate Professor of Radiation Oncology, Department of Radiation Oncology, Mayo Clinic Arizona, 5777 E. Mayo Boulevard, Phoenix, AZ 85054; Liu.Wei@mayo.edu.

*Co-first authors who contributed equally to this work.

Conflicts of Interest Notification

Dr. Terence T. Sio provides strategic and scientific recommendations as a member of the Advisory Board and speaker for Novocure, Inc., which is not in any way associated with the content or disease site as presented in this review.

Other authors have no financial or non-financial interests to be declared.

Ethical considerations

This research was approved by the Mayo Clinic Arizona Institutional Review Board (IRB No. 13–005709). The informed consent was waived by IRB protocol. Only image and dose-volume data were used in this study. All patient-related health information was removed after completion of this study.

Results: The developed comprehensive plan robustness tool had been successfully applied to compare the plan robustness between 3D and 4D robustly optimized IMPT plans for 10 lung cancer patients. In the presence of interplay effect with uncertainties considered simultaneously, 4D robustly optimized plans provided significantly better CTV coverage ($D_{95\%}$, p=0.002), CTV homogeneity ($D_{5\%}$-$D_{95\%}$, p=0.002) with less target hot spots ($D_{5\%}$, p=0.002), and target coverage robustness (CTV $D_{95\%}$ bandwidth, p=0.004) compared to 3D robustly optimized plans. Superior dose sparing of normal lung (lung D_{mean}, p=0.020) favoring 4D plans and comparable normal tissue sparing including esophagus, heart, and spinal cord for both 3D and 4D plans were observed. The calculation time for all patients included in this study was 11.4±2.6 minutes.

Conclusion: A comprehensive plan robustness evaluation tool was successfully developed and benchmarked for plan robustness evaluation in the presence of interplay effect, setup and range uncertainties. The very high efficiency of this tool marks its clinical adaptation highly practical and versatile, including possible real-time intra-fractional interplay effect evaluation as a potential application for future use.

1. Introduction

Intensity-modulated proton therapy (IMPT) provides dosimetric benefits when treating various tumors as compared to conventional photon therapy[1–4]. However, it is more sensitive to changes of water equivalent depths penetrated by proton beams compared to passive scattering proton therapy and intensity-modulated X-ray based radiation therapy[5–7]. Robust optimization and robustness evaluation methods that consider patient setup and proton range uncertainties have been studied by multiple groups and adopted in clinical practice[2,8–28]. A robustly optimized plan may better spare organs at risk (OARs) while providing acceptable target coverage under perturbed scenarios (robustness) compared to the conventional planning target volume (PTV)-based methods[9,15,20].

In addition to patient setup and proton range uncertainties, the targets and patient anatomy (air, lung parenchyma, and mediastinal soft tissue) is constantly changing due to respiratory motion when treating lung cancer. Therefore, interplay effect resulting from the interference between the time-dependent spot delivery and tumor motion should be considered. Studies have shown that interplay effect degrades the dose distribution significantly[29–41]. They can be assessed by simulating the temporal relationship between the spot delivery and patients' respiratory motion and evaluating the resulting dose distribution.

However, most of studies published so far about interplay effect evaluation were assuming that patients' respiratory motion was regular and would breathe exactly with the same breathing pattern during the treatment course as observed in the 4D-CT simulation. In fact, respiratory motion can be irregular and unpredictable, especially in lung cancer patients with compromised pulmonary function and past smoking history[42]. The respiratory period may vary from cycle to cycle within any given treatment session and from day to day during the treatment course[43]. The relative time spent in each phase in one cycle may also change (or so-called asymmetric breathing)[43–45]. Respiratory motion pattern changes may happen such as the respiratory amplitude variations and the baseline drift due to hysteresis[46] during the patient treatment. Thus, a large number of uncertainties may be involved in the evaluation of

interplay effect. In addition, the resulting dose distribution is also affected by setup and range uncertainties. Therefore, it is important to consider the impact from both breathing and treatment uncertainties in the plan robustness evaluation simultaneously[47,48]. This comprehensive plan robustness evaluation would generate dose distributions that are more representative of the actual dose delivered in patients, providing more realistic dosimetric data for IMPT plan evaluation. Unfortunately this important topic has been rarely reported in the literature.

Recently, a number of studies have been performed using IMPT to treat lung cancer with 4D robust optimization[19,49–52] instead of the previous 3D robust optimization without breathing motion considered[19,49,51–53]. The 4D robust optimization involves full 4D-CT-based planning, while 3D robust optimization is planned on 4D averaged CTs. Previous investigations have found that 4D robust optimization achieved an IMPT plan more resilient to interplay effect compared to 3D robust optimization in lung cancer treated by IMPT[19]. Unfortunately, in that reported study, the impacts of uncertainty and interplay effect were considered separately in the plan robustness evaluation. More importantly, interplay effect evaluation was performed with regular respiratory motion only. A comprehensive evaluation of plan robustness is needed for accessing the impact from both treatment uncertainties and interplay effect with irregular respiratory motion considered simultaneously for 4D robust optimization compared to 3D robust optimization. If plausible, the dual evaluation plan will serve as one excellent example of application to benchmark the comprehensive plan robustness evaluation tool if such a tool has been developed.

In this study, we developed a comprehensive plan robustness evaluation tool that considered interplay effect under irregular respiratory motion and treatment uncertainties simultaneously to achieve a more realistic estimation of the delivered dose. Benchmarking the tool as an application's example, we used the developed tool to compare the plan robustness of 3D vs. 4D robustly optimized IMPT plans in lung cancer.

2. Materials and methods

2.1 Development of the comprehensive plan robustness evaluation method

2.1.1 Modelling patient setup and proton range uncertainties—To evaluate the plan robustness to patient setup and proton range uncertainties, we calculated the dose distributions in randomly sampled scenarios with patient setup and proton range uncertainties (Figure 1a). The setup uncertainty was modeled by shifting the iso-center of the patient in the Anterior-Posterior (A-P), Superior-Inferior (S-I), and Right-Left (R-L) directions. The shifted displacement was modelled by a Gaussian distribution with zero mean and a standard deviation of 2.5 mm in all directions. The proton range uncertainty was simulated by scaling the CT number conversion relative to water-stopping-power ratios, which was again modelled by a Gaussian distribution with zero mean and a standard deviation of 1.75%. The standard derivations of both Gaussian distributions for plan robustness evaluation were determined as half of the values that were used in plan optimization (see Sec. 2.2.2).

2.1.2 Post-processing spot-repainting considerations—The iso-layer repainting procedure was used to mitigate interplay effects and was considered in all comprehensive plan robustness evaluations[10–12,18]. The minimum and maximum MU limits of our proton beam delivery system were considered in the repainting procedure as follows. For a spot with intensity larger than the maximum MU limit, it would be split into multiple spots, which would be appended to the end of the spot list in the same energy layer to be re-painted ultimately. For a spot with planned intensity less than the minimum MU limit, by checking whether its intensity is larger or smaller than the half of the minimum MU limit, its intensity would be rounded up to be the minimum MU limit, or otherwise be dropped. Therefore, not all of the spots with intensities smaller than the minimum MU limits are ignored; on the contrary, some of those spots might be assigned a larger intensity to compensate for the dropped spots. Thus the loss of the total MU is generally negligible. All of the appended spots were delivered after delivering all spots of the same energy layer.

In practice, we also adopted a patient-specific maximum MU limits for repainting according to patients' respiratory amplitude that were measured in 4D-CT (listed in the seventh column of Table 1). If the respiratory motion was greater than 5 mm, a smaller maximum MU limit of 0.01 MU was used to provide more repainting; otherwise a larger maximum MU limit of 0.04 MU was applied. The energy-dependent number of protons per MU was defined according to IAEA TRS 398 during the absolute dosimetry commissioning for our commercial treatment planning system (TPS). The minimum and maximum MU limits used in the post-processing have been carefully designed to minimize the resulting plan quality degradation during the commissioning of our commercial TPS.

2.1.3 Modelling patients' respiratory motion—In this study, we investigated the impact of irregular breathing motion upon interplay effect but limited to asymmetric breathing and/or respiratory period variations[43–45]. We did not consider respiration amplitude variation or baseline drift[46]. Structural change from respiratory motion was captured by 4D-CT during the patient simulation. 4D-CT data is obtained from a low-pitch helical[54,55] CT scan that oversamples each couch position and a simultaneously-recorded real-time position management system (RPM) (Varian Medical Systems, Palo Alto, CA). The phase from the RPM data was used to sort CT slices into 3D images of the respiratory cycle in 10 phases (*i.e.*, phase-based sorting[54–57] was used). Thus every respiratory cycle was divided equally into 10 phases. To simulate the irregularity in patient breathing pattern, we analyzed the breathing pattern data from RPM. During patients' 4D-CT simulations, 40 to 50 respiratory cycles were usually scanned, although patients' respiratory periods varied from cycle to cycle (Figure 1b). The respiratory cycle of every patient was modelled as a normal distribution with two patient-specific parameters: the mean and standard deviation of the respiratory cycle, which can be easily derived based on the 40 to 50 respiratory cycles from the corresponding patient's RPM data during the 4D-CT simulation before the treatment. The breathing length for each phase of every patient was 1/10 of the respiratory cycle sampled based on the aforementioned patient-specific normal distribution. One respiratory cycle would be formed after 10 sampling: each sampling corresponding to one of the ten phases within one respiratory cycle. The respiratory cycle thus generated would have

the breathing length varying from phase to phase (or so-called asymmetric breathing)[43–45]. Details of the parameters were listed in Table 2.

2.1.4 Interplay effect evaluation—We used the characteristics of the proton machine at our hospital including energy layer switching time, dose rate, spill length, spill interval length, and spot interval length to model the time structure of spot delivery (Hitachi ProbeatV5, with detailed parameters listed in Table 3)[58]. To simulate interplay effect, the final dose (referred as 4D dynamic dose hereafter) was computed by simulating the accumulated dose through this delivery process (Figure 1b). Each spot was temporarily registered to a phase according to the temporal relationship between patients' breathing patterns and the time-dependent spot delivery process determined by the proton machine characteristics. Dose received on each phase was calculated using the spots assigned to that phase and its corresponding 4D-CT using an in-house-developed dose calculation engine[59]. These phase-specific doses were finally deformed to a reference phase (the maximum exhalation phase, T50) using deformable image registration[60], and the 4D dynamic dose was obtained by summing doses from all phases. Interplay effect was then evaluated by comparing the 4D dynamic dose with the 4D cumulative dose (see the definition in Sec. 2.2.2). For each field per fraction, randomization of the initial phase by evenly selecting one of the 10 possible phases modeled by a uniform distribution was performed.

2.1.5 Evaluation with patient setup, range uncertainties, and interplay effect considered simultaneously—To evaluate plan robustness of a treatment plan, we considered the impact of interplay effect with uncertainties considered simultaneously. For uncertainties, we sampled a total of 30 uncertainty scenarios with setup and range uncertainties considered for each plan as described in Sec. 2.1.1 (Figure 1a). For each uncertainty scenario, an influence matrix, indicating the contribution of each spot of unit weight to every voxel, was calculated and stored in the computer memory for efficient subsequent dose computation. For every uncertainty scenario, we derived 10 possible 4D dynamic dose distributions corresponding to 10 asymmetric breathing patterns. Each of the 10 irregular motion pattern includes tens to a hundreds of respiratory traces. The number of the respiratory traces for each irregular motion pattern equals to the number of fraction times the number of fields (*i.e.*, for each fraction of each field, a different respiratory trace independently sampled as described in Sec. 2.1.3 will be used). The temporal length of each respiratory trace is sufficiently long for the delivery of the corresponding field for the corresponding fraction (the delivery time is modeled as in Sec. 2.1.4) with randomized initial phase (described in Sec. 2.1.4). For example, for a patient treated with 3 field and 30 fractions, 90 respiratory traces will be simulated for each irregular motion pattern. The initial phase will be sampled 90 times in this case. If the patient has a mean respiratory period of 3 seconds and 90 seconds are needed to delivery one field, each respiratory trace will have at least 30 respiratory cycles. The related interplay effect was evaluated by calculating the corresponding 4D dynamic doses as described in Sec. 2.1.4.

Dose-volume histogram (DVH) curves were generated for each calculated 4D dynamic dose distribution. With 30 uncertainty scenarios considered for every asymmetric breathing scenario, a total of 300 DVHs were computed for each treatment plan to represent the

possible perturbed doses in the presence of both uncertainties and interplay effect (Figure 1c). In this study, we used the DVH band method[20,61–63] for plan robustness quantification, in which all DVHs from the corresponding perturbed scenarios were plotted, and the width of the envelope from all DVHs was used as an indication of plan robustness (Figure 1d). The narrower the DVH band, the more robust the treatment plan would be. Details of the sampling variables in this comprehensive plan robustness evaluation are listed in Table 2.

2.2 Application of the developed method to compare the plan robustness between 3D and 4D robustly optimized plans for lung cancer

Lung cancer treatment was extremely vulnerable to respiratory motions and uncertainties. Although previous evaluation indicated a superior plan robustness of 4D robustly optimized plans than that of 3D robustly optimized plans in lung cancer[19], no plan robustness assessment has been performed under combined effect from both treatment uncertainties and interplay effect with irregular respiratory motions. Here, we evaluated the overall comprehensive robustness of 3D and 4D robustly optimized IMPT plans in lung cancer using the developed tool for clinical application.

2.2.1 Patient selection—In this study, we performed plan robustness evaluation using our novel method on 10 non–small cell lung cancer (NSCLC) patients who had been treated at our hospital, and re-planned them for IMPT using 3D and 4D robust optimizations. The spot sizes (σ) in air at the isocenter were 6–14 mm, depending on energy. The patients were not consecutively selected based on clinical volumes, but rather were carefully chosen to represent varying tumor stages, target volumes, and respiratory motion patterns (Table 1) so that the cases sampled by our method represented a comprehensive clinical experience. The statistics such as mean, median, standard deviation, and range for the patient cohort was shown in Supplementary Table 1.

2.2.2 Development of 3D and 4D robustly optimized IMPT plans—For each patient, one 3D robustly optimized plan (3D-RO) and one 4D robustly optimized (4D-RO) plan were generated with identical dosimetric goals by our in-house GPU-accelerated TPS as described in Sec. 2.3. The number of spots and their positions before optimization were the same for both 3D and 4D robust optimization. The prescription dose, number of fractions, tumor location, stage, target size, beam angles, proton energy, and repainting information are reported in Table 1.

The 3D robustly optimized plans were generated using the voxel-wise worst-case robust optimization method with the 4D-averaged CTs as the planning CTs[16]. Thirteen (13) uncertainty scenarios of setup and range uncertainty (5 mm rigid shift in all Anterior-Posterior [A-P], Superior-Inferior [S-I], and Right-Left [R-L] directions combining ±3.5% proton range rescaling, as a total of 12 scenarios, plus one nominal scenario) were considered. The setup and range uncertainties were set twice as much as those used in the robustness evaluation (σ = (2.5mm, ±1.75%)), for deriving the worst-case scenario in plan optimizations[7,15,20,63]. The CTV's at the exhalation phase (CTV_{T50}) were contoured by experienced thoracic radiation oncologists and then propagated to other phases. All the other OARs were contoured by the experienced dosimetrists and verified by the treating radiation

oncologists on the average 4D-CT. The optimization target was set to be the internal target volume (ITV), which was formed by consideration to motion extents of the clinical target volumes (CTV) using all phases of the 4D-CT's. The details regarding the 3D robust optimization process and workflow for proton lung cancer in our practice have previously been published[10]

The 4D robustly optimized plans were generated using the 4D robust optimization method described in Liu *et al.*[19]. Note that no irregular respiratory motion was considered in the 4D robust optimization. The 4D CTs were used as the planning CT with the CTV_{T50} as the optimization target. In this case, the same aforementioned 13 scenarios of setup and range uncertainty were considered for every respiration phase without interplay effect considered during the plan optimization. Computed dose distributions for the 10 phases were accumulated to the reference phase (T50) using deformed image registration to get the 4D cumulative dose for all 13 uncertainty scenarios. 4D cumulative dose represents an equally-weighted dose accumulation from all respiratory phases. The voxel-wise worst-case dose distribution among 13 4D cumulative dose distributions was then generated and optimized to generate the 4D robustly optimized IMPT plan.

The post-processing procedure as described in Sec. 2.1.2 was not considered in the 3D and 4D plan optimization, but was considered in the comprehensive plan robustness evaluation as described in Sec. 2.1. The minimum MU limit (0.003 MU) of our machine was carefully chosen to minimize the possible plan degradation due to the post processing. The median and range of repainting number among all energy layers from 3D and 4D robustly optimized plans of all patients were listed in the eleventh and twelfth column of Table 1, and details in Supplementary Table 2.

2.2.3 Plan quality evaluation—The 4D cumulative dose distributions as described in Sec. 2.2.2 of both 3D and 4D robustly optimized plans of each patient were calculated. The 4D cumulative dose for all plans was checked to ensure that the institutional dose-volume constraints were met (Table 4). The 3D robustly optimized plan was normalized to have the same CTV $D_{95\%}$ (the dose covering the hottest 95% of the structure's volume) as the 4D robustly optimized plans for fair comparisons.

After normalization, both 3D and 4D robustly optimized plans were evaluated with both uncertainties and interplay effect simultaneously considered as described in Sec. 2.1.5. The 4D cumulative and 4D dynamic doses from both plans were used for plan evaluation.

$D_{95\%}$ (the dose covering the hottest 95% of the structure's volume) was derived from the CTV_{T50} DVH to evaluate the target coverage. CTV_{T50} $D_{5\%}$ and $D_{5\%}$-$D_{95\%}$ were also used to assess CTV hot spots and homogeneity. The absolute dose covering certain percentage of the structure's volume ($D_{\%}$) was compared for organs at risk (OARs). We used $D_{1\%}$ dose for the spinal cord and $D_{33\%}$ dose to the esophagus. In addition, the mean dose (D_{mean}) to the total normal lung and heart were also used.

2.3 Graphic Processing Unit (GPU)-accelerated treatment planning system

A large number of time-consuming computations were needed for this study. In order to speed up the calculation, we migrated our in-house developed treatment planning system (TPS) to a Graphic Processing Unit (GPU)-based computing platform, including the following 3 components: (1) a modified ray-casting-based dose and linear energy transfer (LET) calculation engine[59,64], with the enhanced capability to account for inhomogeneity more accurately[65]; (2) voxel-wise worst-case-based 3D[10,12–17,20,25–28,66–69], 4D[19], and LET-guided[26,70] robust optimization; and (3) DVH-band method[20,61,63] to quantify plan robustness. The TPS was highly parallelized using Compute Unified Device Architecture (CUDA). Dose calculations for a typical patient could typically be completed within 20 seconds and one 3D robust optimization within several minutes running on Intel Xeon® CPU E5–2680 CPU equipped with 8 Tesla K80s (Nvidia, Santa Clara, California). The dose calculation results from our TPS agreed well with Monte Carlo-based dose calculation results (Supplementary Table 3). The details of this GPU-accelerated TPS will be reported in a separate study.

2.4 Statistical Considerations

All DVH evaluation metrics as described in Sec. 2.2.3 were compared with the non-parameter Wilcoxon signed rank test, using Matlab 2019a (MathWorks, Massachusetts, USA). A p-value of <0.05 was considered statistically significant.

3. Results

We first compared the 4D cumulative doses in the nominal scenario (no uncertainties or interplay effect considered) of both 3D and 4D robustly optimized plans. Compared to the 3D robustly optimized plans, the 4D robustly optimized plans achieved better target homogeneity in the nominal scenario (CTV $D_{5\%}$-$D_{95\%}$: 0.050 vs 0.024 [3D vs 4D robustly optimized plans, normalized to nominal $D_{95\%}$ dose, for all CTV-related quantification later on], p=0.006, Figure 2a). We also examined the normal tissue sparing of both 3D and 4D robustly optimized plans. Compared to 3D robustly optimized plans, better lung sparing was observed from 4D robustly optimized plans (lung D_{mean}: 9.48 Gy[RBE] vs 9.16 Gy[RBE] [3D vs 4D robustly optimized plans, absolute dose, for all OAR-related quantification later on], p=0.027). Comparable dose distributions to esophagus (esophagus $D_{33\%}$: 20.79 Gy[RBE] vs 20.82 Gy[RBE], p=0.131), spinal cord (spinal cord $D_{1\%}$: 16.69 Gy[RBE] vs 16.01 Gy[RBE], p=0.770), and heart (heart D_{mean}: 2.42 Gy[RBE] vs 2.46 Gy[RBE], p=0.846) were observed (Figure 3a).

To investigate the impact from interplay effect with uncertainties considered simultaneously, we studied the 4D dynamic dose distributions from all 10 patients for both the 3D and 4D robustly optimized plans (as described in Sec. 2.1.5). The worst-case dose derived from the 300 sampled scenarios was used for comparison. In the worst-case scenario, 4D robustly optimized plans showed significant improvements in CTV coverage (CTV $D_{95\%}$, 0.913 vs 0.979, p=0.002), CTV dose homogeneity (CTV $D_{5\%}$-$D_{95\%}$, 0.158 vs 0.050, p=0.002), and reduction in hot spots (CTV $D_{5\%}$, 1.072 vs 1.030, p=0.002) for all 10 cases (Figure 2b). Compared to 3D robustly optimized plans, better sparing of lung (D_{mean}, 9.27 Gy[RBE] vs

8.98 Gy[RBE], p=0.020) and comparable dose distributions in esophagus ($D_{33\%}$, 24.20 Gy[RBE] vs 22.90 Gy[RBE], p=0.232), spinal cord ($D_{1\%}$: 31.21 Gy[RBE] vs 29.93 Gy[RBE], p=0.695) and heart (D_{mean}: 4.30 Gy[RBE] vs 4.53 Gy[RBE], p=0.492) from 4D robustly optimized plans were observed (Figure 3b).

We further studied plan robustness by quantifying the bandwidth of those DVH indices from the calculated 300 scenarios. Compared to 3D robustly optimized plan, 4D robustly optimized plans had improved target coverage robustness (CTV $D_{95\%}$ bandwidth, 0.090 vs 0.048, p=0.004) and comparable hot-spot insensitivity (CTV $D_{5\%}$ bandwidth, 0.035 vs 0.033, p=0.846) to uncertainties and interplay effect, and thus, appeared more robust (Figure 2c). Otherwise, no significant difference in plan robustness to multiple OARs was observed (esophagus $D_{33\%}$ bandwidth, 8.63 Gy[RBE] vs 6.87 Gy[RBE], p=0.492; spinal cord $D_{1\%}$ bandwidth: 16.96 Gy[RBE] vs 15.89 Gy[RBE], p=0.557; lung D_{mean} bandwidth, 6.33 Gy[RBE] vs 6.25 Gy[RBE], p=0.625; heart D_{mean} bandwidth: 5.92 Gy[RBE] vs 6.85 Gy[RBE], p=0.106) (Figure 3c).

Figure 4 illustrates the axially calculated dose distribution of one typical patient (patient #2) near the inferior pole of the tumor. Without uncertainties or interplay effect considered, the 4D cumulative dose distribution (top row) of the 3D robustly optimized plan (left column) was outperformed by the 4D robustly optimized plan (right column). With uncertainties and interplay effect simultaneously considered (bottom row, displaying one out of the 300 scenarios), the target coverage dropped substantially for the 3D robustly optimized plan but was mostly maintained for the 4D robustly optimized plan (minimum CTV $D_{95\%}$ of 300 4D dynamic doses, 0.870 vs. 0.969).

The average total computation time for evaluating one plan was 11.4 minutes with a standard deviation of 2.6 min for all 10 patients included in this study. Individual computation times for each patient are listed in Table 5.

4. Discussion

We have successfully developed a comprehensive plan robustness evaluation tool to consider the impact of interplay effect, setup, and range uncertainties simultaneously. As an example of application, we used the developed tool to compare the performance of 3D and 4D robustly optimized plans for 10 lung cancer patients on a GPU-accelerated computing platform. Without sacrificing the dose coverage of the target, the 4D robustly optimized plans significantly reduced the target hotspot (CTV $D_{5\%}$) and increased the target homogeneity (CTV $D_{5\%}$-$D_{95\%}$) in the nominal scenario without uncertainties and interplay effect considered. Compared to the nominal scenario, the target coverage (CTV $D_{95\%}$) of both 3D and 4D robustly optimized plans was significantly degraded (p= 0.002 for both 3D and 4D plans) in the presence of uncertainties and interplay effect (comparing first panels of Figure 2a and 2b). However, significantly better target coverage was observed comparing the 4D robustly optimized plans to the 3D robustly optimized plans (p= 0.002), suggesting an enhanced mitigation effect against the plan quality deterioration due to uncertainties and interplay effect comparing 4D robust optimization to 3D robust optimization (Figure 4).

Compared to the 3D robustly optimized plans, 4D robustly optimized plans showed improvements in tumor coverage (average CTV $D_{95\%}$ increased from 91.3% to 97.9%, p=0.002), tumor dose homogeneity (average CTV $D_{5\%}$- $D_{5\%}$ decreased from 0.158 to 0.050, p=0.002), and reduction of hot spot distributions (averaged CTV $D_{5\%}$ decreased from 1.072 to 1.030, p=0.002) in the worst-case scenario with uncertainties and interplay effect considered simultaneously. 4D robustly optimized plans also achieved superior plan robustness in tumor coverage compared to 3D robustly optimized plans ($D_{95\%}$ bandwidth decreased from 0.090 to 0.048, p=0.004). These observations are consistent with previous studies with the impact of uncertainties and interplay effect considered independently[19], supporting the validity of the proposed comprehensive plan robustness evaluation method. Generally, both 3D and 4D robustly optimized plans achieved similar normal tissue sparing and plan robustness in OARs. However, compared to 3D robustly optimized plans, 4D robustly optimized plans delivered significantly lower mean doses to normal lung. This would potentially reduce the risk of radiation pneumonitis, pending clinical correlative studies in the future[71,72].

We developed this comprehensive plan robustness evaluation tool by simultaneously assessing the impact from both uncertainties and interplay effect. Different from the previous plan robustness evaluation approach using Monte Carlo simulation[48], we demonstrated clinical applications of our current method on 10 patients by comparing performance between 3D and 4D robustly optimized plans for non-small cell lung cancer. With the help of fast GPU-based computation platform and effective implementation of parallelization using CUDA, we significantly speeded up the calculation of interplay effect, which used to be a technical barrier in the interplay effect evaluation when uncertainties were simultaneously considered[19]. Therefore, we were able to calculate 300 scenarios (10 different breathing patterns with 30 uncertainty scenario considered for each breathing pattern) for each plan very quickly. Among the 10 different breathing patterns, irregular respiratory motion was modelled by parameters derived from patient-specific RPM data[73]. The average total computation time for evaluating one plan with 300 uncertainty scenarios was 11.4 minutes, substantially reduced compared to the estimated 1,500 to 3,000 hours running on a non-GPU-accelerated computing platform if 300 scenarios based on 10 respiratory phases were considered. This new software implementation that is GPU computational platform-based may be able to perform real-time, intrafractional evaluation daily for patients undergoing IMPT treatments by using the delivery log-file data on the proton machine[74,75].

We evaluated the interplay effect by mimicking machine delivery procedure and patient's breathing patterns as much as possible. The machine delivery is modelled based on the proton machine characteristics at our proton center. In the current practice, the reconstruction of 4D-CT based on equally-divided respiratory phase[54–57] or respiratory amplitude[76–78] can be problematic and could introduce imperfection in the reconstructed images and consequentially impact the interplay effect evaluation. In addition, we simulated irregular breathing patterns from patient-specific RPM data with varying breathing length of each phase only (or so-called asymmetric breathing)[43–45]. This method does not consider the possible respiratory motion pattern changes such as the respiratory amplitude variations and the baseline drift due to hysteresis that may occur during the patient's treatment. More

precise models may help perfect this method by including these variables in the future. The respiratory amplitude variation can be modelled by scaling of the magnitude in the deformable vector fields, and the baseline drift can be simulated by shifting the tumor position accordingly.

Our current interplay effect evaluation from breathing motion is based on 4DCT. More sophisticated representation of patient breathing motion can be achieved using new techniques such as cine-MRI[79–82] or 4D MRI[83–85] with finer time resolution. These MRI based approaches provide more precise respiratory motion modelling and therefore the resulting anatomical changes. The 4D dynamic dose calculation method based on the synthetic 4D CT-MRI has been used for interplay effect evaluation with irregular respiratory motion considered[86]. With the technique becoming available to us, we will adapt our mathematical models according to these new data in the future.

It is important to validate the accuracy of the tool by phantom measurements. However, experimentally validating and benchmarking such a tool can be challenging. To mimic the realistic clinical scenario as much as possible, an inhomogeneous phantom with complicated 3D target motion, rather than 1D translational motion, is needed[87,88]. This is a subject for further research by our group in the future. For more comprehensive tests of the software, other proton plans generated by different methods such as using Monte Carlo dose engine, based on proton machines by other vendors, with different delivery techniques such as single field optimization (SFO), etc. should be considered. This will be included in the future studies as well.

This developed tool has certain limitations. To reduce the evaluation time required, we used the same values for both range and setup uncertainties (30 combined scenarios) for every fraction. In reality, the patient setup uncertainties may behave more randomly from fraction to fraction during the treatment course. Although the approximation to consider patient setup uncertainties being the same for every fraction may overestimate the actual impact due to setup uncertainty, we had 30 randomized setup and range uncertainty considered and covered. The result, therefore, may reasonably represent most, if not all, of the possible perturbations from these uncertainties throughout the entire treatment course. It would be beneficial if a more efficient dose calculation computational approach can be developed in the future. Besides, additional uncertainties from inter-fractional anatomic changes are not considered in the current method, along with its potential induced motion variations. Further studies are warranted to evaluate the impact of these anatomic changes possibly by taking into account repeated weekly 4D CTs in the current method or by on-line real time interplay effects evaluation using on-board volumetric imaging. This will be considered in a follow-on study.

We presented a new tool to evaluate interplay effect with uncertainties considered simultaneously. This evaluation method may be adopted in a new 4D robust optimization strategy[51,52,89] by optimizing the worst-case dose distribution from this comprehensive plan robustness evaluation method. The resulting new 4D robust optimization method can potentially generate IMPT plans more resilient to irregular respiratory motion in an effective manner.

5. Conclusion

We have successfully developed a new plan robustness evaluation tool by accessing interplay effect with uncertainties considered simultaneously in IMPT for non-small cell lung cancer treatments, accounting for irregular respiratory motion modelled by parameters derived from patient-specific RPM data. We validated this method using 10 lung cancer patients and compared the plan robustness between 3D and 4D robustly optimized plans. Improved plan quality and robustness were achieved using 4D robust optimization. The proposed method may provide clinicians with comprehensive assessment of plan robustness in the presence of interplay effect and setup and range uncertainties, and thus enabling more realistic estimation of the delivered dose in IMPT for thoracic radiotherapy applications.

Supplementary Material

Refer to Web version on PubMed Central for supplementary material.

Acknowledgments

This research was supported by the National Cancer Institute (NCI) Career Developmental Award K25CA168984, Arizona Biomedical Research Commission Investigator Award, the Lawrence W. and Marilyn W. Matteson Fund for Cancer Research, and the Kemper Marley Foundation.

Dr. Wei Liu reports grants from NIH/NCI, grants from Arizona Department of Health Science, grants from The Lawrence W. and Marilyn W. Matteson Fund for Cancer Research, grants from The Kemper Marley Foundation, outside the submitted work; In addition, The LET calculation technology reported in this study has been licensed to .decimal LLC by Mayo Clinic.

Dr. Schild reports “write and edit for UpToDate”.

References

1. Register SP, Zhang X, Mohan R, Chang JY. Proton stereotactic body radiation therapy for clinically challenging cases of centrally and superiorly located stage I non-small-cell lung cancer. International Journal of Radiation Oncology*Biology*Physics. 2011;80:1015–1022.
2. Stuschke M, Kaiser A, Pottgen C, Lubcke W, Farr J. Potentials of robust intensity modulated scanning proton plans for locally advanced lung cancer in comparison to intensity modulated photon plans. Radiotherapy and oncology : journal of the European Society for Therapeutic Radiology and Oncology. 2012;104(1):45–51. [PubMed: 22560714]
3. Zhang X, Li Y, Pan X, et al. Intensity-modulated proton therapy reduces the dose to normal tissue compared with intensity-modulated radiation therapy or passive scattering proton therapy and enables individualized radical radiotherapy for extensive stage IIIB non-small-cell lung cancer: a virtual clinical study. International journal of radiation oncology, biology, physics. 2010;77.
4. Schild SE, Rule WG, Ashman JB, et al. Proton beam therapy for locally advanced lung cancer: A review. World journal of clinical oncology. 2014;5(4):568–575. [PubMed: 25302161]
5. Lomax AJ. Intensity modulated proton therapy and its sensitivity to treatment uncertainties 1: the potential effects of calculational uncertainties. Physics in Medicine and Biology. 2008;53(4):1027–1042. [PubMed: 18263956]
6. Lomax AJ. Intensity modulated proton therapy and its sensitivity to treatment uncertainties 2: the potential effects of inter-fraction and inter-field motions. Physics in Medicine and Biology. 2008;53(4):1043–1056. [PubMed: 18263957]
7. Lomax AJ. Intensity modulated proton therapy: the potential and the challenge [Habilitation Thesis] Zurich: Department of Physics, ETH; 2004.

8. Chen W, Unkelbach J, Trofimov A, et al. Including robustness in multi-criteria optimization for intensity-modulated proton therapy. Physics in Medicine and Biology. 2012;57(3):591–608. [PubMed: 22222720]
9. Fredriksson A, Forsgren A, Hardemark B. Minimax optimization for handling range and setup uncertainties in proton therapy. Medical Physics. 2011;38(3):1672–1684. [PubMed: 21520880]
10. Liu C, Sio TT, Deng W, et al. Small-spot intensity-modulated proton therapy and volumetric-modulated arc therapies for patients with locally advanced non-small-cell lung cancer: A dosimetric comparative study [published online ahead of print 2018/10/18]. J Appl Clin Med Phys. 2018;19(6):140–148. [PubMed: 30328674]
11. Liu C, Yu NY, Shan J, et al. Technical Note: Treatment planning system (TPS) approximations matter - comparing intensity-modulated proton therapy (IMPT) plan quality and robustness between a commercial and an in-house developed TPS for nonsmall cell lung cancer (NSCLC) [published online ahead of print 2019/09/10]. Med Phys. 2019. doi: 10.1002/mp.13809.
12. Liu CB, Schild SE, Chang JY, et al. Impact of Spot Size and Spacing on the Quality of Robustly Optimized Intensity Modulated Proton Therapy Plans for Lung Cancer. International Journal of Radiation Oncology Biology Physics. 2018;101(2):479–489.
13. Liu W, Frank SJ, Li X, et al. Effectiveness of Robust Optimization in Intensity-Modulated Proton Therapy Planning for Head and Neck Cancers. Med Phys. 2013;40(5):051711–051718. [PubMed: 23635259]
14. Liu W, Frank SJ, Li X, Li Y, Zhu RX, Mohan R. PTV-based IMPT optimization incorporating planning risk volumes vs robust optimization. Medical Physics. 2013;40(2):021709–021708. [PubMed: 23387732]
15. Liu W, Li Y, Li X, Cao W, Zhang X. Influence of robust optimization in intensity-modulated proton therapy with different dose delivery techniques. Med Phys. 2012;39.
16. Liu W, Liao Z, Schild SE, et al. Impact of respiratory motion on worst-case scenario optimized intensity modulated proton therapy for lung cancers. Practical Radiation Oncology. 2015;5(2):e77–86. [PubMed: 25413400]
17. Liu W, Mohan R, Park P, et al. Dosimetric benefits of robust treatment planning for intensity modulated proton therapy for base-of-skull cancers. Practical Radiation Oncology. 2014;4:384–391. [PubMed: 25407859]
18. Liu W, Patel SH, Harrington DP, et al. Exploratory study of the association of volumetric modulated arc therapy (VMAT) plan robustness with local failure in head and neck cancer [published online ahead of print 2017/05/16]. J Appl Clin Med Phys. 2017;18(4):76–83.
19. Liu W, Schild SE, Chang JY, et al. Exploratory Study of 4D versus 3D Robust Optimization in Intensity Modulated Proton Therapy for Lung Cancer. International Journal of Radiation Oncology Biology Physics. 2016;95(1):523–533.
20. Liu W, Zhang X, Li Y, Mohan R. Robust optimization in intensity-modulated proton therapy. Med Phys. 2012;39:1079–1091. [PubMed: 22320818]
21. Pflugfelder D, Wilkens JJ, Oelfke U. Worst case optimization: a method to account for uncertainties in the optimization of intensity modulated proton therapy. Physics in Medicine and Biology. 2008;53(6):1689–1700. [PubMed: 18367797]
22. Unkelbach J, Bortfeld T, Martin BC, Soukup M. Reducing the sensitivity of IMPT treatment plans to setup errors and range uncertainties via probabilistic treatment planning. Medical Physics. 2009;36(1):149–163. [PubMed: 19235384]
23. Unkelbach J, Chan TCY, Bortfeld T. Accounting for range uncertainties in the optimization of intensity modulated proton therapy. Physics in Medicine and Biology. 2007;52(10):2755–2773. [PubMed: 17473350]
24. Liu W, Li Y, Li X, Cao W, Zhang X. Influence of robust optimization in intensity-modulated proton therapy with different dose delivery techniques Med Phys. 2012;39(6):3089–4001 [PubMed: 22755694]
25. An Y, Liang JM, Schild SE, Bues M, Liu W. Robust treatment planning with conditional value at risk chance constraints in intensity- modulated proton therapy. Medical Physics. 2017;44(1):28–36. [PubMed: 28044325]

26. An Y, Shan J, Patel SH, et al. Robust intensity-modulated proton therapy to reduce high linear energy transfer in organs at risk. Medical Physics. 2017;44(12):6138–6147. [PubMed: 28976574]
27. Shan J, An Y, Bues M, Schild SE, Liu W. Robust optimization in IMPT using quadratic objective functions to account for the minimum MU constraint. Medical Physics. 2018;45(1):460–469. [PubMed: 29148570]
28. Shan J, Sio TT, Liu C, Schild SE, Bues M, Liu W. A novel and individualized robust optimization method using normalized dose interval volume constraints (NDIVC) for intensity-modulated proton radiotherapy [published online ahead of print 2018/11/06]. Med Phys. 2018. doi: 10.1002/mp.13276.
29. Kraus KM, Heath E, Oelfke U. Dosimetric consequences of tumor motion due to respiration for a scanned proton beam. Phys Med Biol. 2011;56:6563–6581. [PubMed: 21937770]
30. Phillips MH, Pedroni E, Blattmann H, Boehringer T, Coray A, Scheib S. EFFECTS OF RESPIRATORY MOTION ON DOSE UNIFORMITY WITH A CHARGED-PARTICLE SCANNING METHOD. Phys Med Biol. 1992;37(1):223–234. [PubMed: 1311106]
31. Lambert J, Suchowerska N, McKenzie DR, Jackson M. Intrafractional motion during proton beam scanning. Physics in Medicine and Biology. 2005;50(20):4853–4862. [PubMed: 16204877]
32. Grozinger SO, Bert C, Haberer T, Kraft G, Rietzel E. Motion compensation with a scanned ion beam: a technical feasibility study. Radiation Oncology. 2008;3. [PubMed: 18190681]
33. Seco J, Robertson D, Trofimov A, Paganetti H. Breathing interplay effects during proton beam scanning: simulation and statistical analysis. Phys Med Biol. 2009;54(14):N283–N294. [PubMed: 19550002]
34. Grozinger SO, Rietzel E, Li Q, Bert C, Haberer T, Kraft G. Simulations to design an online motion compensation system for scanned particle beams. Physics in Medicine and Biology. 2006;51(14):3517–3531. [PubMed: 16825746]
35. Dowdell S, Grassberger C, Sharp GC, Paganetti H. Interplay effects in proton scanning for lung: a 4D Monte Carlo study assessing the impact of tumor and beam delivery parameters. Physics in Medicine and Biology. 2013;58(12):4137–4156. [PubMed: 23689035]
36. Grassberger C, Dowdell S, Lomax A, et al. Motion Interplay as a Function of Patient Parameters and Spot Size in Spot Scanning Proton Therapy for Lung Cancer. International Journal of Radiation Oncology Biology Physics. 2013;86(2):380–386.
37. Knopf A-C, Hong TS, Lomax A. Scanned proton radiotherapy for mobile targets-the effectiveness of re-scanning in the context of different treatment planning approaches and for different motion characteristics. Physics in Medicine and Biology. 2011;56(22):7257–7271. [PubMed: 22037710]
38. Li Y, Kardar L, Li X, et al. On the interplay effects with proton scanning beams in stage III lung cancer. Medical Physics. 2014;41(2).
39. Kardar L, Li Y, Li X, et al. Evaluation and mitigation of the interplay effects of intensity modulated proton therapy for lung cancer in a clinical setting. Practical Radiation Oncology. 2014;4(6):e259–268. [PubMed: 25407877]
40. Bortfeld T, Jokivarsi K, Goitein M, Kung J, Jiang SB. Effects of intra-fraction motion on IMRT dose delivery: statistical analysis and simulation. Phys Med Biol. 2002;47(13):2203–2220. [PubMed: 12164582]
41. Matney J, Park PC, Bluett J, et al. Effects of Respiratory Motion on Passively Scattered Proton Therapy Versus Intensity Modulated Photon Therapy for Stage III Lung Cancer: Are Proton Plans More Sensitive to Breathing Motion? International Journal of Radiation Oncology Biology Physics. 2013;87(3):576–582.
42. Yamamoto T, Langner U, Loo BW, Shen J, Keall PJ. RETROSPECTIVE ANALYSIS OF ARTIFACTS IN FOUR-DIMENSIONAL CT IMAGES OF 50 ABDOMINAL AND THORACIC RADIOTHERAPY PATIENTS. International Journal of Radiation Oncology Biology Physics. 2008;72(4):1250–1258.
43. Chan TCY, Bortfeld T, Tsitsiklis JN. A robust approach to IMRT optimization. Physics in Medicine and Biology. 2006;51(10):2567–2583. [PubMed: 16675870]
44. Bortfeld T, Chan TCY, Trofimov A, Tsitsiklis JN. Robust Management of Motion Uncertainty in Intensity-Modulated Radiation Therapy. Operations Research. 2008;56(6):1461–1473.

45. Chan TCY, Misic VV. Adaptive and robust radiation therapy optimization for lung cancer. European Journal of Operational Research. 2013;231(3):745–756.
46. Heath E, Unkelbach J, Oelfke U. Incorporating uncertainties in respiratory motion into 4D treatment plan optimization. Medical Physics. 2009;36(7):3059–3071. [PubMed: 19673205]
47. Pepin MD, Tryggestad E, Wan Chan Tseung HS, Johnson JE, Herman MG, Beltran C. A Monte-Carlo-based and GPU-accelerated 4D-dose calculator for a pencil beam scanning proton therapy system [published online ahead of print 2018/09/12]. Med Phys. 2018;45(11):5293–5304. [PubMed: 30203550]
48. Souris K, Barragan Montero A, Janssens G, Di Perri D, Sterpin E, Lee JA. Technical Note: Monte Carlo methods to comprehensively evaluate the robustness of 4D treatments in proton therapy [published online ahead of print 2019/08/04]. Med Phys. 2019;46(10):4676–4684. [PubMed: 31376305]
49. Yu J, Zhang X, Liao L, et al. Motion-robust intensity-modulated proton therapy for distal esophageal cancer. Medical Physics. 2016;43(3):1111–1118. [PubMed: 26936698]
50. Pfeiler T, Ahmad Khalil D, Bäumer C, et al. 4D robust optimization in pencil beam scanning proton therapy for hepatocellular carcinoma. Journal of Physics: Conference Series. 2019;1154:012021.
51. Bernatowicz K, Zhang Y, Perrin R, Weber DC, Lomax AJ. Advanced treatment planning using direct 4D optimisation for pencil-beam scanned particle therapy [published online ahead of print 2017/06/22]. Phys Med Biol. 2017;62(16):6595–6609. [PubMed: 28635614]
52. Engwall E, Fredriksson A, Glimelius L. 4D robust optimization including uncertainties in time structures can reduce the interplay effect in proton pencil beam scanning radiation therapy [published online ahead of print 2018/07/18]. Med Phys. 2018. doi: 10.1002/mp.13094.
53. Unkelbach J, Alber M, Bangert M, et al. Robust radiotherapy planning. Physics in Medicine & Biology. 2018;63(22):22TR02.
54. Ford EC, Mageras GS, Yorke E, Ling CC. Respiration-correlated spiral CT: A method of measuring respiratory-induced anatomic motion for radiation treatment planning. Med Phys. 2003;30(1):88–97. [PubMed: 12557983]
55. Vedam S, Keall P, Kini V, Mostafavi H, Shukla H, Mohan R. Acquiring a four-dimensional computed tomography dataset using an external respiratory signal. Phys Med Biol. 2002;48(1):45.
56. Rietzel E, Pan T, Chen GTY. Four-dimensional computed tomography: Image formation and clinical protocol. Med Phys. 2005;32(4):874–889. [PubMed: 15895570]
57. Wolthaus JW, Sonke J-J, van Herk M, et al. Comparison of different strategies to use four-dimensional computed tomography in treatment planning for lung cancer patients. International Journal of Radiation Oncology* Biology* Physics. 2008;70(4):1229–1238.
58. Shen J, Tryggestad E, Younkin JE, et al. Technical Note: Using experimentally determined proton spot scanning timing parameters to accurately model beam delivery time [published online ahead of print 2017/08/05]. Med Phys. 2017;44(10):5081–5088. [PubMed: 28777447]
59. Younkin JE, Morales DH, Shen J, et al. Clinical Validation of a Ray-Casting Analytical Dose Engine for Spot Scanning Proton Delivery Systems [published online ahead of print 2019/11/23]. Technol Cancer Res Treat. 2019;18:1533033819887182. [PubMed: 31755362]
60. Wang H, Dong L, O'Daniel J, et al. Validation of an accelerated 'demons' algorithm for deformable image registration in radiation therapy. Physics in Medicine and Biology. 2005;50(12):2887–2905. [PubMed: 15930609]
61. Trofimov A, Kang J, Unkelbach J, et al. Evaluation of dosimetric gain and uncertainties in proton therapy delivery with scanned pencil beam in treatment of base-of-skull and spinal Tumors. International Journal of Radiation Oncology Biology Physics. 2010;78(3):S133–S134.
62. Liu W, ed Robustness quantification and robust optimization in intensity-modulated proton therapy Springer; 2015 Rath A, Sahoo N, eds. Particle Radiotherapy: Emerging Technology for Treatment of Cancer.
63. Liu W, Patel SH, Shen JJ, et al. Robustness quantification methods comparison in volumetric modulated arc therapy to treat head and neck cancer. Practical Radiation Oncology. 2016;6(6):E269–E275. [PubMed: 27025166]

64. Deng W, Ding X, Younkin JE, et al. Hybrid 3D analytical linear energy transfer calculation algorithm based on precalculated data from Monte Carlo simulations [published online ahead of print 2019/11/24]. Med Phys. 2019. doi: 10.1002/mp.13934.

65. Soukup M, Fippel M, Alber M. A pencil beam algorithm for intensity modulated proton therapy derived from Monte Carlo simulations. Physics in Medicine and Biology. 2005;50(21):5089–5104. [PubMed: 16237243]

66. Liu C, Bhangoo RS, Sio TT, et al. Dosimetric comparison of distal esophageal carcinoma plans for patients treated with small-spot intensity-modulated proton versus volumetric-modulated arc therapies [published online ahead of print 2019/05/22]. J Appl Clin Med Phys. 2019;20(7):15–27. [PubMed: 31112371]

67. Liu C, Yu NY, Shan J, et al. Technical Note: Treatment planning system (TPS) approximations matter - comparing intensity-modulated proton therapy (IMPT) plan quality and robustness between a commercial and an in-house developed TPS for nonsmall cell lung cancer (NSCLC) [published online ahead of print 2019/09/10]. Med Phys. 2019;46(11):4755–4762. [PubMed: 31498885]

68. Zhang P, Fan N, Shan J, Schild SE, Bues M, Liu W. Mixed integer programming with dose-volume constraints in intensity-modulated proton therapy [published online ahead of print 2017/07/07]. J Appl Clin Med Phys. 2017;18(5):29–35. [PubMed: 28681976]

69. Zaghian M, Lim G, Liu W, Mohan R. An Automatic Approach for Satisfying Dose-Volume Constraints in Linear Fluence Map Optimization for IMPT [published online ahead of print 2014/12/17]. J Cancer Ther. 2014;5(2):198–207. [PubMed: 25506501]

70. Liu C, Patel SH, Shan J, et al. Robust Optimization for Intensity-Modulated Proton Therapy to Redistribute High Linear Energy Transfer (LET) from Nearby Critical Organs to Tumors in Head and Neck Cancer [published online ahead of print 2020/01/29]. International journal of radiation oncology, biology, physics. 2020. doi: 10.1016/j.ijrobp.2020.01.013.

71. Yu NY, DeWees TA, Liu C, et al. Early Outcomes of Patients With Locally Advanced Non-small Cell Lung Cancer Treated With Intensity-Modulated Proton Therapy Versus Intensity-Modulated Radiation Therapy: The Mayo Clinic Experience. Advances in Radiation Oncology. doi: 10.1016/j.adro.2019.08.001.

72. Tejan Diwanji AS, Terence T. Sio, Nirav V Patel, Pranshu Mohindra. Proton stereotactic body radiation therapy for non-small cell lung cancer. Annals of Translational Medicine. 2020. doi: 10.21037/atm-20-2975.

73. Ribeiro CO, Meijers A, Korevaar EW, et al. Comprehensive 4D robustness evaluation for pencil beam scanned proton plans [published online ahead of print 2019/04/25]. Radiotherapy and oncology : journal of the European Society for Therapeutic Radiology and Oncology. 2019;136:185–189. [PubMed: 31015123]

74. Fattori G, Klimpki G, Hrbacek J, et al. The dependence of interplay effects on the field scan direction in PBS proton therapy [published online ahead of print 2019/03/21]. Phys Med Biol. 2019;64(9):095005. [PubMed: 30893664]

75. Hernandez Morales D, Shan J, Liu W, et al. Automation of routine elements for spot-scanning proton patient-specific quality assurance [published online ahead of print 2018/10/20]. Med Phys. 2019;46(1):5–14. [PubMed: 30339270]

76. Wink NM, Panknin C, Solberg TD. Phase versus amplitude sorting of 4D-CT data. J Appl Clin Med Phys. 2006;7(1):77–85. [PubMed: 16518319]

77. Vásquez A, Runz A, Echner G, Sroka-Perez G, Karger C. Comparison of two respiration monitoring systems for 4D imaging with a Siemens CT using a new dynamic breathing phantom. Phys Med Biol. 2012;57(9):N131. [PubMed: 22504160]

78. Low DA, Nystrom M, Kalinin E, et al. A method for the reconstruction of four-dimensional synchronized CT scans acquired during free breathing. Med Phys. 2003;30(6):1254–1263. [PubMed: 12852551]

79. Sawant A, Keall P, Pauly KB, et al. Investigating the feasibility of rapid MRI for image-guided motion management in lung cancer radiotherapy [published online ahead of print 2014/02/14]. BioMed research international. 2014;2014:485067. [PubMed: 24524077]

80. Kumar S, Liney G, Rai R, Holloway L, Moses D, Vinod SK. Magnetic resonance imaging in lung: a review of its potential for radiotherapy. The British Journal of Radiology. 2016;89(1060):20150431. [PubMed: 26838950]

81. Arai TJ, Nofiele J, Madhuranthakam AJ, et al. Characterizing spatiotemporal information loss in sparse-sampling-based dynamic MRI for monitoring respiration-induced tumor motion in radiotherapy [published online ahead of print 2016/06/10]. Med Phys. 2016;43(6):2807–2820. [PubMed: 27277029]

82. Garau N, Via R, Meschini G, et al. A ROI-based global motion model established on 4DCT and 2D cine-MRI data for MRI-guidance in radiation therapy [published online ahead of print 2019/01/10]. Phys Med Biol. 2019;64(4):045002. [PubMed: 30625459]

83. Bernatowicz K, Peroni M, Perrin R, Weber DC, Lomax A. Four-Dimensional Dose Reconstruction for Scanned Proton Therapy Using Liver 4DCT-MRI [published online ahead of print 2016/04/17]. International journal of radiation oncology, biology, physics. 2016;95(1):216–223.

84. Boye D, Lomax T, Knopf A. Mapping motion from 4D-MRI to 3D-CT for use in 4D dose calculations: A technical feasibility study. Medical Physics. 2013;40(6).

85. Meschini G, Vai A, Paganelli C, et al. Virtual 4DCT from 4DMRI for the management of respiratory motion in carbon ion therapy of abdominal tumors [published online ahead of print 2019/12/28]. Med Phys. 2020;47(3):909–916. [PubMed: 31880819]

86. Dolde K, Zhang Y, Chaudhri N, et al. 4DMRI-based investigation on the interplay effect for pencil beam scanning proton therapy of pancreatic cancer patients. Radiation Oncology. 2019;14(1):30. [PubMed: 30732657]

87. Ehrbar S, Perrin R, Peroni M, et al. Respiratory motion-management in stereotactic body radiation therapy for lung cancer - A dosimetric comparison in an anthropomorphic lung phantom (LuCa). Radiotherapy and Oncology. 2016;121(2):328–334. [PubMed: 27817945]

88. Perrin RL, Zakova M, Peroni M, et al. An anthropomorphic breathing phantom of the thorax for testing new motion mitigation techniques for pencil beam scanning proton therapy. Physics in Medicine and Biology. 2017;62(6):2486–2504. [PubMed: 28240218]

89. Buti G, Souris K, Montero AMB, Lee JA, Sterpin E. Towards fast and robust 4D optimization for moving tumors with scanned proton therapy [published online ahead of print 2019/10/09]. Med Phys. 2019;46(12):5434–5443. [PubMed: 31595521]

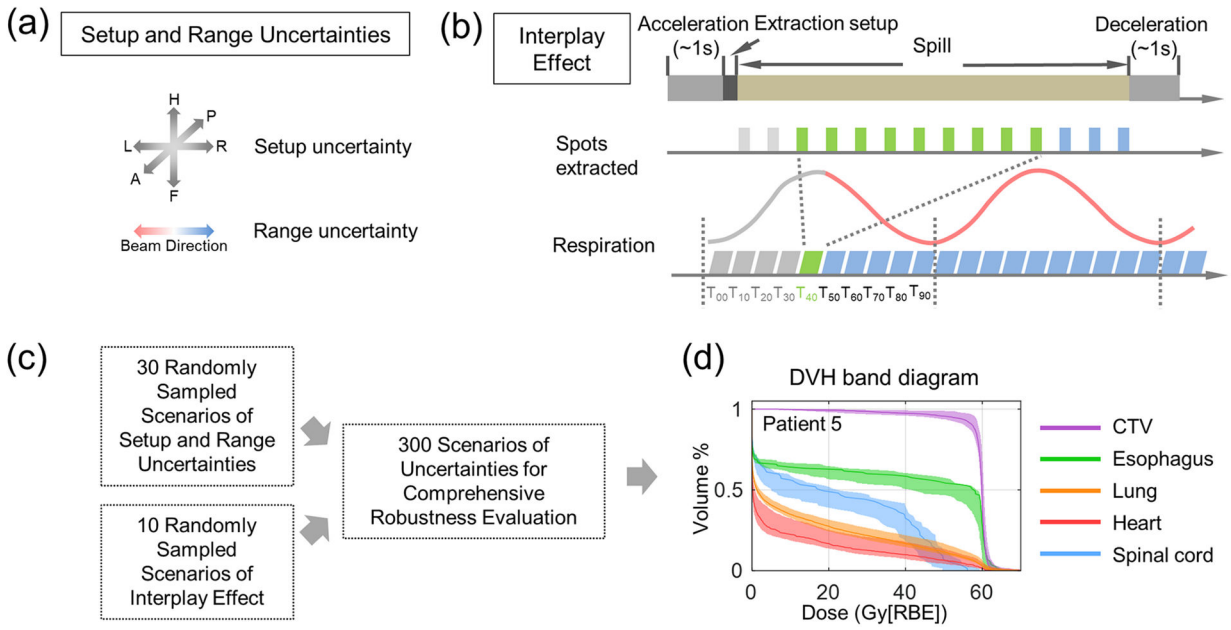

Figure 1. Diagram and workflow of comprehensive robustness evaluation.

a) Setup and range uncertainties were modelled by shifting the patient's iso-center and rescaling the proton range; b) Interplay effect was simulated by evaluating the interference between spot delivery and respiratory motions; c) The comprehensive plan robustness was evaluated by calculating interplay effect with the impact of both uncertainties considered; d) DVH-band graph derived from 300 combined scenarios for each plan that was used for plan robustness evaluation.

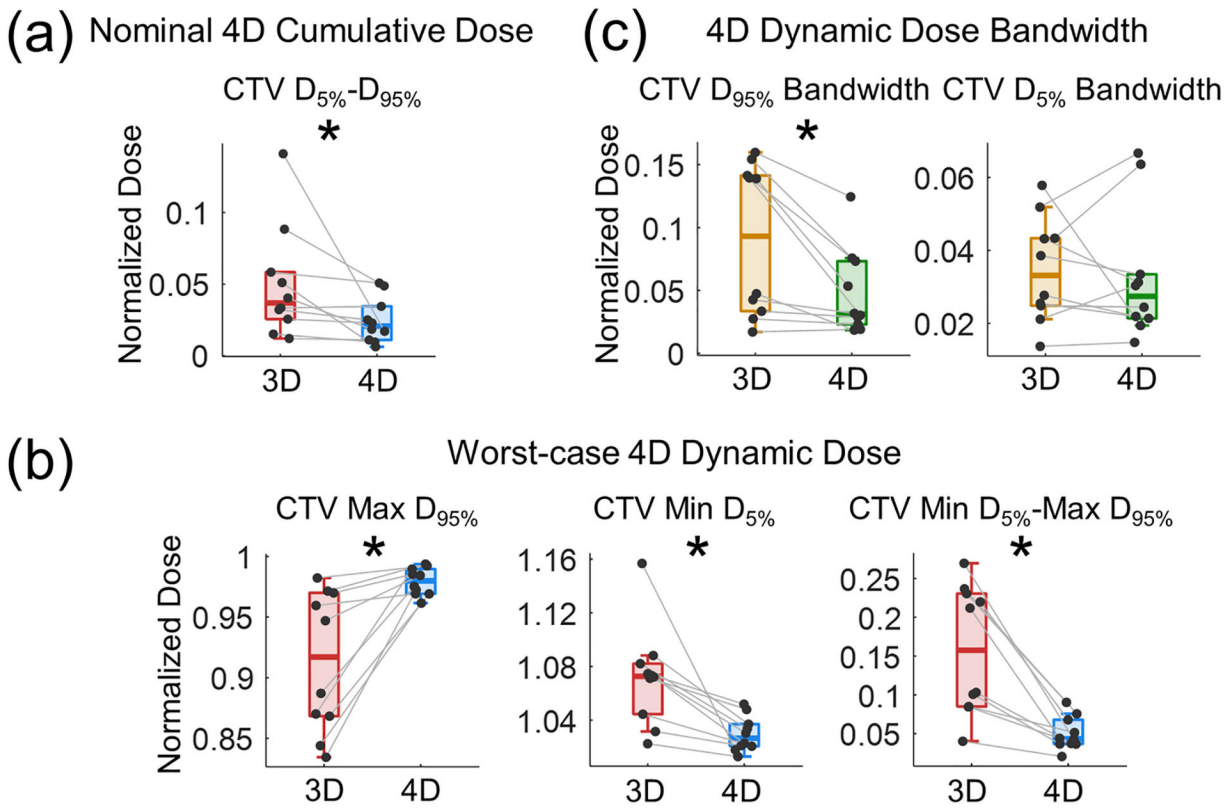

Figure 2. Comparisons of 3D and 4D robustly optimized plans for the IMPT targets.

a) Box-and-scatter plot of $D_{5\%}$-$D_{95\%}$ CTV 4D cumulative doses from 10 patients for both 3D and 4D robustly optimized plans in the nominal scenario; b) Box-and-scatter plot of 4D dynamic doses of CTV $D_{95\%}$, $D_{5\%}$, and $D_{5\%}$-$D_{95\%}$ from 10 patients for both 3D and 4D robustly optimized plans in the worst-case scenario; c) Box-and-scatter plot of bandwidth for $D_{95\%}$ and $D_{5\%}$ derived from the 300 calculated 4D dynamic dose scenerios of 10 patients for both 3D and 4D robustly optimized plans. * indicates $p<0.05$.

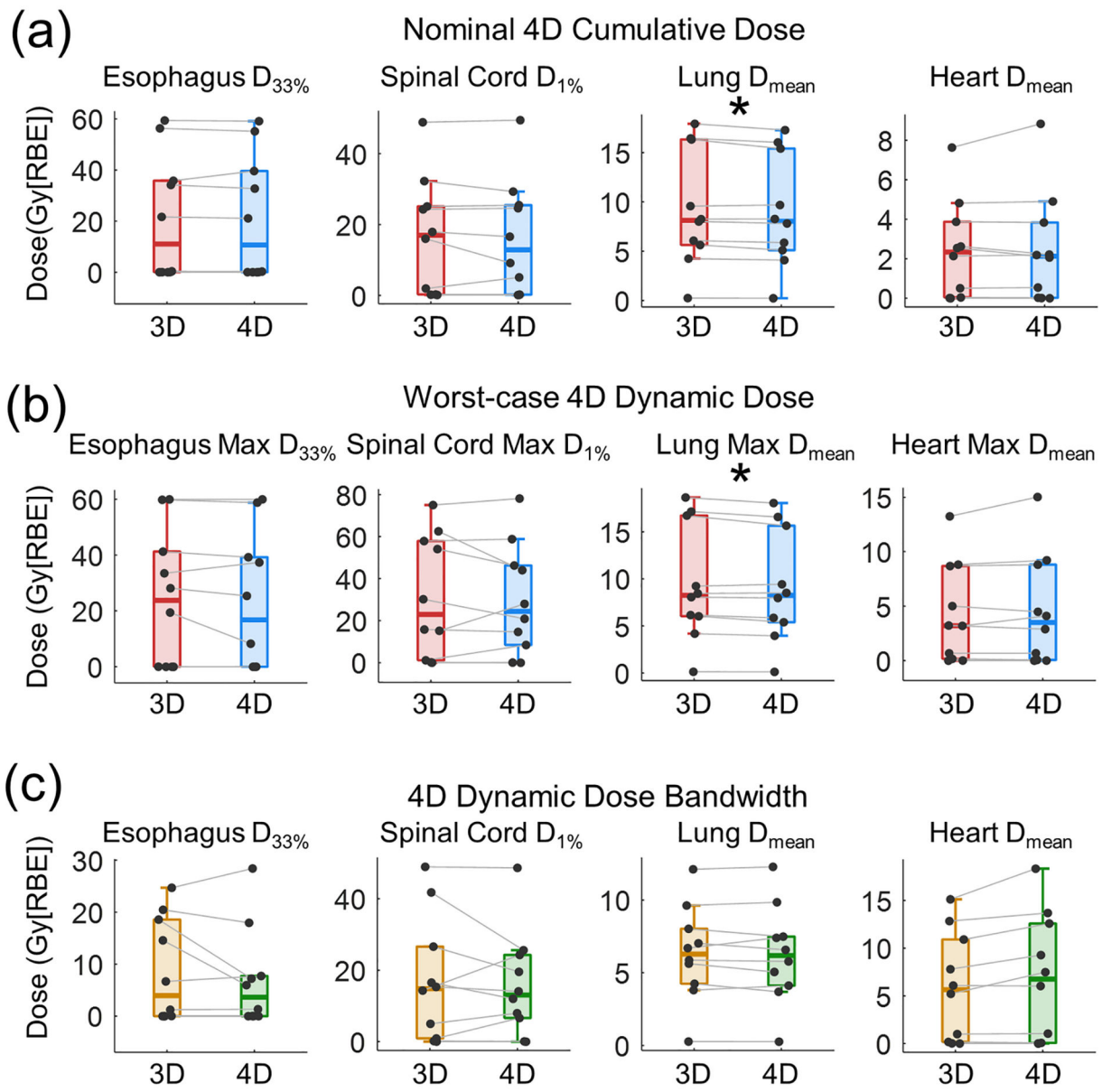

Figure 3. Comparisons of 3D and 4D robustly optimized plans for OARs.

a) Box-and-scatter plot of 4D cumulative dose of esophagus $D_{33\%}$, spinal cord $D_{1\%}$, lung mean dose and heart mean dose from 10 patients for both 3D and 4D robustly optimized plans in the nominal scenario; b) Box-and-scatter plot of 4D dynamic doses of esophagus $D_{33\%}$, spinal cord $D_{1\%}$, lung mean dose and heart mean dose from 10 patients for both 3D and 4D robustly optimized plans in the worst-case scenario; c) Box-and-scatter plot of bandwidth of esophagus $D_{33\%}$, spinal cord $D_{1\%}$, lung mean dose and heart mean dose derived from 300 4D dynamic doses of 10 patients for both 3D and 4D robustly optimized plans. * indicates $p<0.05$.

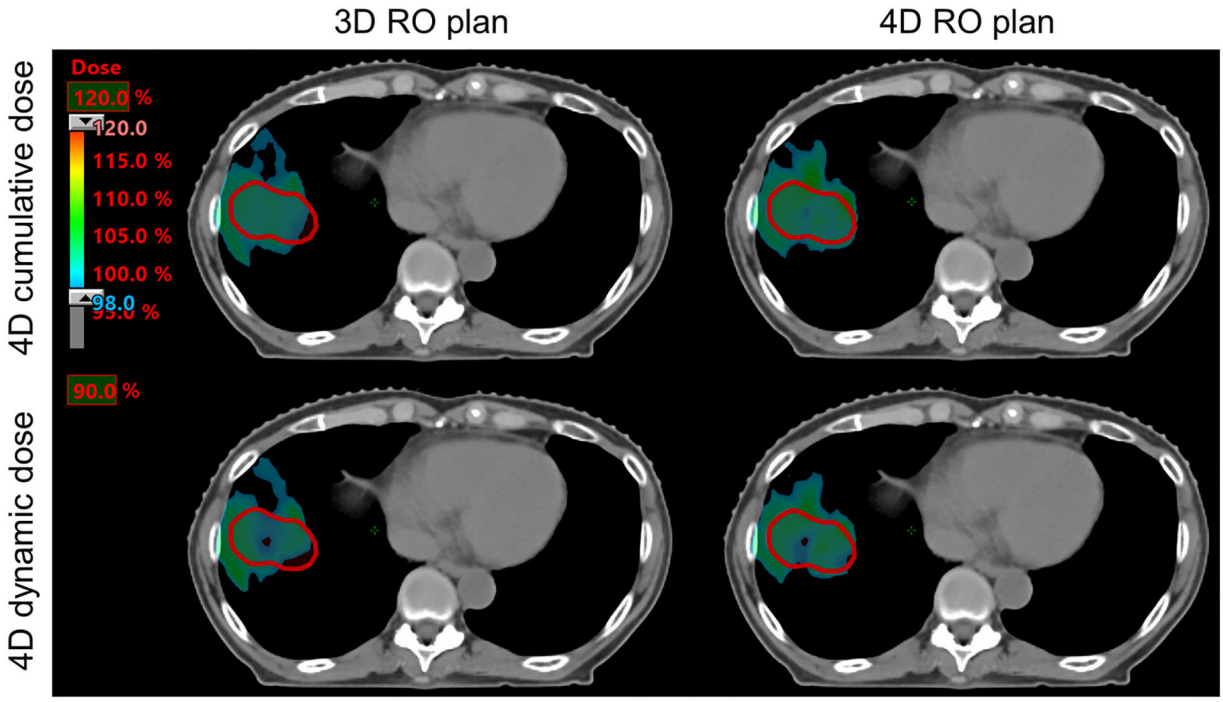

Figure 4. Doses (in color wash presentation) for the 98% prescription iso-dose distribution comparison between a 3D robustly optimized plan (left column) and a 4D robustly optimized plan (right column).

The top row shows the 4D cumulative doses in the nominal scenario. The bottom row shows the 4D dynamic doses with the presence of both uncertainties and interplay effect considered simultaneously; the red lines contour represents the CTV.

Table 1

Patient, Tumor, and IMPT Plan Parameter Characteristics for 10 NSCLC Patients

Pat.#	Prescrip. Dose (Gy[RBE])	Fx[a]	Tumor Loc.	Stage	Target Size (cc)	RMA[b] (mm)	Beam Angles of Gantry and Couch (°)	Energy Range (MeV)	Energy Layer #	Repainting # Among All Energy Layers (med.(range))		Delivery Duration (sec)
										3D RO	4D RO	
1	40	5	Lower right	I	14.5	7	180, 180	118.4–151.9	29	5(2–10)	3(1–7)	89.8
							155, 180	122.3–158.3	30	3(1–8)	2(1–13)	91.7
2	60	30	Lower right	IIIB	282.2	11	35, 180	91.7–148.1	44	9(1–37)	9(1–36)	107.7
							165, 180	109.1–175.6	48	6.5(1–42)	7(1–20)	111.6
							0, 180	94.8–151.9	45	7(1–24)	8.5(1–27)	110.9
3	50	20	Lower left	IIB	130.5	7	180, 180	83.7–137.9	41	2(1–18)	2(1–3)	93.9
							155, 0	86.9–141.4	42	4.5(1–19)	2(1–5)	102.8
4	60	30	Lower left	IIIA	76.1	9	165, 180	93.2–147.0	42	8(3–44)	6(1–37)	96.5
							155, 0	94.8–146.2	41	11(3–22)	9(2–62)	107.9
							77, 0	86.9–137.9	39	5(2–19)	6(2–26)	91.9
5	60	30	Upper right	IIIC	248.5	11	40, 180	97.8–159.9	48	6(1–39)	7(1–60)	108.4
							30, 0	106.4–159.9	42	3.5(1–37)	3(1–67)	90
							155, 180	129.7–200.4	44	12(2–31)	10(1–34)	119.9
							180, 180	127.2–193.6	43	8(1–49)	8(1–61)	118.8
6	60	30	Lower right	IIIA	64.1	7.5	150, 180	96.3–155.1	47	4(1–20)	3(1–21)	101.3
							185, 180	94.8–149.2	44	3(1–8)	2(1–12)	95.5
7	60	30	Lower left	IIIA	291.4	9	180, 270	71.3–140.2	50	4(1–7)	4(1–8)	125.9
							100, 0	80.3–175.6	68	3(1–5)	3(1–6)	154.2
8	60	30	Middle right	IIIB	388.6	8	70, 180	73.2–177.5	73	8(1–16)	7(1–15)	195.3
							160, 180	91.7–183.3	65	4(1–15)	3(1–16)	176.6
9	60	30	Upper left	IIIA	181.2	4.5	155, 0	90.1–151.9	49	1(1–5)	1(1–4)	118.7
							170, 180	83.7–155.1	55	2(1–4)	2(1–5)	131
10	60	15	Upper left	IB	114.4	7.1	20, 0	71.3–141.4	51	3(1–18)	3(1–14)	129
							170, 180	83.7–146.2	48	4(1–13)	2.5(1–12)	121
							100, 0	122.3–169.6	36	2(1–8)	2(1–7)	98.9

[a] Fx: Fractions;

[b] RMA: Respiratory motion amplitude

Table 2

Summary of parameters for comprehensive robustness evaluation

Uncertainty Type		Distribution	Parameter	Sampling frequency	Number of uncertainty cases
Setup and range uncertainties	Setup	Normal	$\mu = 0$; $\sigma = 2.5$ mm	Once per course	30
	Range	Normal	$\mu = 0$; $\sigma = 1.75\%$	Once per course	
Interplay effect	Initial respiratory phase	Uniform	Phase 1 to Phase 10	Once per field per fraction	10
	Breathing length of respiratory phase	Normal	μ = patient-specific mean length of respiration cycle; σ = 18% of patient-specific mean length of respiration cycle *	Once per respiratory phase	

* Since most of patients included in this study were treated a long time ago, the associated RPM data acquired during the initial 4D CT simulations for these patients were deleted (per our institution policy, the RPM data would only be stored in the 4D CT simulator for 3 months); only the mean lengths of respiratory cycles of these patients were available to us. We analyzed the RPM data for 40 patients currently available to us and found that roughly the ratio of the standard deviation over mean length of patients' respiratory cycles was 18%. Thus we had set the patient-specific standard deviation of patients' respiratory cycles to be 18% of patient-specific mean length of respiratory cycles for every patient included in this study. We believe that this assumption would not affect our final conclusions.

Table 3

Proton Machine Characteristics for Spot Delivery as Used in IMPT Planning

Parameters	Values
Spot Size (In-air at Isocenter)	Energy-dependent (σ: 2–6 mm)
Spot Spacing	5 mm
Minimum MU Limit (MU[a])	0.003
Maximum MU Limit (MU[a])	0.04
Energy Layer Switching Time (s)	1.9
Spill Length (s)	7.9
Effective Magnet Scanning Speed in Horizontal Direction, V_x (m/s)	Medium Energy Group: 5.7
	Low Energy Group: 7.0
Effective Magnet Scanning Speed in Vertical Direction, V_y (m/s)	High Energy Group: 17.1
	Medium Energy Group: 18.2
	Low Energy Group: 22.2
Magnet Preparation/Verification Time (ms[b])	1.93
Proton Spill Rate (MU[a]/s)	High Energy Group: 9.8
	Medium Energy Group: 8.1
	Low Energy Group: 8.5

[a]MU: Monitor Unit;

[b]ms: Millisecond;

Table 4

Suggested Dose-Volume Constraints for Conventionally Fractionated Thoracic IMPT Planning

Target/Critical structure	Dose limits (Gy) or Constraint Goals
Clinical target volume	> 99% volume receiving > 95% of the prescription dose in the worst-case scenario
Brachial plexus	Minimum dose to 0.03 cc highest dose volume < 60 Gy[RBE]
Esophagus	1/3 volume < 65 Gy[RBE]; 2/3 volume < 55 Gy[RBE], as low as reasonably achievable
Liver	Mean dose to liver < 25 Gy[RBE]; 1/3 liver < 35 Gy[RBE]
Total lung	Mean lung dose < 20 Gy[RBE], $V_{20\ Gy[RBE]}$ < 37% of volume
Spinal cord	Maximum dose to 0.03cc highest dose volume < 50 Gy[RBE]
Heart	1/3 volume < 60 Gy[RBE]; 2/3 volume < 45 Gy[RBE]; mean heart dose < 30 Gy[RBE], as low as reasonably achievable

Table 5

Average Total Computation Time for Plan Evaluation

Patient #	Calculation time (min)
1	13.0
2	9.2
3	10.9
4	7.1
5	14.8
6	9.7
7	10.9
8	10.3
9	12.3
10	15.4